

Magnetic ordering in the XY pyrochlore antiferromagnet $\text{Er}_2\text{Ti}_2\text{O}_7$: a spherical neutron polarimetry study

This article has been downloaded from IOPscience. Please scroll down to see the full text article.

2007 *J. Phys.: Condens. Matter* 19 452201

(<http://iopscience.iop.org/0953-8984/19/45/452201>)

[View the table of contents for this issue](#), or go to the [journal homepage](#) for more

Download details:

IP Address: 129.252.86.83

The article was downloaded on 29/05/2010 at 06:30

Please note that [terms and conditions apply](#).

FAST TRACK COMMUNICATION

Magnetic ordering in the XY pyrochlore antiferromagnet $\text{Er}_2\text{Ti}_2\text{O}_7$: a spherical neutron polarimetry study

A Poole^{1,2}, A S Wills^{1,2,4} and E Lelièvre-Berna³

¹ Department of Chemistry, University College London, 20 Gordon Street, London WC1H 0AJ, UK

² Davy-Faraday Research Laboratory, The Royal Institution of Great Britain, London W1S 4BS, UK

³ Institut Laue-Langevin, BP 156, 38042 Grenoble Cedex 9, France

E-mail: a.s.wills@ucl.ac.uk

Received 16 July 2007, in final form 28 August 2007

Published 11 October 2007

Online at stacks.iop.org/JPhysCM/19/452201

Abstract

$\text{Er}_2\text{Ti}_2\text{O}_7$ has been proposed as a realization of the $XY\langle 111 \rangle$ pyrochlore antiferromagnet with dipolar interactions, where the spins of Er^{3+} lie perpendicular to the $\langle 111 \rangle$ local axes. Below a Néel temperature of $T_N = 1.173$ K magnetic order with the propagation vector $\vec{k} = (000)$ occurs. Previous powder neutron diffraction studies were not able to determine details of the magnetic ordering beyond its symmetry due to powder averaging. In an attempt to resolve the questions as regards the ordering in this model magnet we performed a spherical neutron polarimetry experiment using CRYOPAD. The analysis of these data and a proposed magnetic order are presented.

(Some figures in this article are in colour only in the electronic version)

One of the central themes in condensed matter research in recent years has been frustration [1, 2], where an inherent competition prevents individual interactions from being satisfied. Its simplest realizations are the so-called geometrically frustrated systems, where the frustration arises from the geometry of the magnetic lattice. Particular interest has been focused on geometries of vertex-sharing triangles and tetrahedra, the *kagomé* and *pyrochlore* lattices, as these possess highly degenerate ground states. Model materials with these structures have been found to display a wide range of exotic low-temperature physics, such as spin ice [3], spin liquid [4, 5], topological spin glass [6, 7], heavy fermion [8], and partially ordered phases [9, 10]. There is an open question in magnetism as regards the influence of anisotropies, as this energy scale is quite distinct from that of the exchange interactions, and may raise, or only partly raise, the degeneracies as well as tuning quantum and thermal fluctuations.

⁴ Author to whom any correspondence should be addressed.

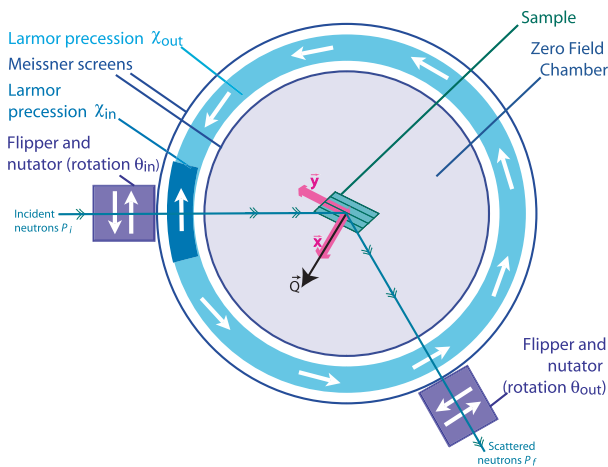


Figure 1. Schematic diagram of the CRYOPAD (cryogenic polarization analysis device) as installed at the ILL. The \bar{x} and \bar{y} orientations of the neutron polarization are marked in relation to \bar{Q} , \bar{z} is out of the page.

The cubic pyrochlore $\text{Er}_2\text{Ti}_2\text{O}_7$ displays a continuous antiferromagnetic ordering transition at $T_N = 1.173$ K despite a relatively large Curie–Weiss temperature $\theta_{\text{CW}} = -22$ K [11], to Néel order with the propagation vector $\vec{k} = 0$ [12]. The 4f^{11} electronic configuration of Er^{3+} gives rise to a $^4\text{I}_{15/2}$ ($L = 6$, $S = 3/2$) single-ion ground state term with a large XY anisotropy that constrains the moments to the local $\langle 111 \rangle$ planes of each tetrahedron. Writing the magnetic representation for the Er^{3+} (16c) as $\Gamma_{\text{Er}} = 1\Gamma_3^{(1)} + 1\Gamma_5^{(2)} + 1\Gamma_7^{(3)} + 2\Gamma_9^{(3)}$, following the numbering scheme of Kovalev [13, 16] where the superscript is the order of the irreducible representation (irrep), powder averaging limited the details determined for the magnetic ordering to its irrep, Γ_5 . The large deviation of the refined moment, $3.0 \mu_B$ at 50 mK, from the $9.59 \mu_B$ expected from the free-ion term is as yet unexplained, but may be related to quantum fluctuations within the Γ_5 manifold. In order to confirm the irrep, and determine the ratio of basis vector coefficients within the irrep, a spherical neutron polarimetry (SNP) experiment was undertaken.

The cubic unit cell of $\text{Er}_2\text{Ti}_2\text{O}_7$ ($Fd\bar{3}m$, $a = 10.04 \text{ \AA}$ at room temperature) contains four symmetry related Er^{3+} ions and those related by the four centring translations. In the following work, the positions of the four Er sites are defined in table 1. The SNP data were taken from an $\sim 8 \text{ mm}^3$ single crystal [12] at $T \sim 50 \text{ mK}$, with the sample mounted within a dilution refrigerator. Measurements were taken with the $\langle \bar{1}10 \rangle$ and $\langle 001 \rangle$ axes vertical. The first orientation allows access to all odd and all even hhl reflections; the second to the $hk0$ set of reflections, where all of the indices are even.

The experiment was carried out using CRYOPAD [14] on the diffractometer D3 at the ILL using polarized neutrons, $\lambda = 0.825 \text{ \AA}$, scattered from a Heusler crystal. These neutrons pass through the incident nutator which changes the direction of the neutron polarization from the beam axis to a chosen transverse direction by an adiabatic rotation of the neutron spins until the polarization direction makes an angle θ with the vertical. The neutrons then pass the precession coils, between the inner and outer Meissner screens, and precess through the angle χ about the horizontal axis. Once past the second Meissner screen the neutrons enter the ‘zero-field’ chamber where they are Bragg diffracted by the lattice planes of the crystal (see figure 1). Each reflection, with scattering vector \vec{Q} , has a related effective magnetic moment described by the magnetic structure factor $\vec{M}(\vec{Q})$. The components of the magnetic moments

Table 1. The basis functions of Γ_5 and Γ_7 for the pyrochlore lattice with the propagation vector $\vec{k} = 0$ and the magnetic atoms at the sites $m_1: (0, 0, 0)$, $m_2: (\frac{1}{2}, \frac{3}{4}, \frac{1}{4})$, $m_3: (\frac{1}{4}, \frac{1}{2}, \frac{3}{4})$, $m_4: (\frac{3}{4}, \frac{1}{4}, \frac{1}{2})$.

irrep	Basis vector	Atom	Basis vector components			Visualization
			a_{\parallel}	b_{\parallel}	c_{\parallel}	
Γ_5	$\vec{\psi}_2$	m_1	2	$\bar{1}$	$\bar{1}$	
		m_2	2	1	1	
		m_3	$\bar{2}$	$\bar{1}$	1	
		m_4	$\bar{2}$	1	$\bar{1}$	
Γ_7	$\vec{\psi}_3$	m_1	0	1	$\bar{1}$	
		m_2	0	$\bar{1}$	1	
		m_3	0	1	1	
		m_4	0	$\bar{1}$	$\bar{1}$	
Γ_7	$\vec{\psi}_4$	m_1	0	1	$\bar{1}$	
		m_2	0	$\bar{1}$	1	
		m_3	0	$\bar{1}$	$\bar{1}$	
		m_4	0	1	1	
Γ_5	$\vec{\psi}_5$	m_1	$\bar{1}$	0	1	
		m_2	1	0	1	
		m_3	1	0	$\bar{1}$	
		m_4	$\bar{1}$	0	$\bar{1}$	
Γ_6	$\vec{\psi}_6$	m_1	1	$\bar{1}$	0	
		m_2	$\bar{1}$	$\bar{1}$	0	
		m_3	1	1	0	
		m_4	$\bar{1}$	1	0	

in the plane perpendicular to \vec{Q} constitute the magnetic interaction vector $\vec{M}(\vec{Q})_{\perp}$ that induces the rotation and further polarization of the neutron beam detected by the analyser. $\vec{M}(\vec{Q})$ and $\vec{M}(\vec{Q})_{\perp} = \vec{Q} \times M(\vec{Q}) \times \vec{Q}$ are generally complex vectors:

$$\vec{M}(\vec{Q}) = \frac{\gamma e^2}{2m_e c^2} \sum_j f(\vec{Q}) \vec{m}_j \exp(i \vec{Q} \cdot \vec{r}_j), \quad (1)$$

where the $\frac{\gamma e^2}{2m_e c^2}$ is a constant with the value 0.269510^{-12} (cm/ μ_B), $f(\vec{Q})$ is the magnetic form factor, and \vec{r}_j is the location of the j th magnetic atom in the unit cell. The moment orientation and magnitude, \vec{m}_j , is the magnitude of the moment, μ , multiplied by the normalized sum over the basis vectors belonging to the i th irrep weighted by the coefficient c_i , $\vec{\Psi}_i = \sum_i c_i \vec{\psi}_i$.

Hence $\vec{m}_j = \mu \sum_j \vec{\Psi}_j / (\vec{\Psi}_j \vec{\Psi}_j^*)$. If the moment size is known, the only free parameters that need to be refined are the coefficients c_i , which have a summed modulus of unity.

The arbitrary direction of the neutron polarization is described using Cartesian coordinates with: the x axis parallel to the scattering vector \vec{Q} ; the z axis vertical and parallel to the zone axis of the crystal; the y axis completing the right-handed set (see figure 1). The x component of $\vec{M}(\vec{Q})_\perp$ is necessarily null.

The neutron spin and effective moment of the metal site need to be described in the same coordinate system in order to calculate values of $\vec{M}(\vec{Q})_\perp$. This can be achieved by converting the axis system of the magnetic structure factor from crystallographic to the Cartesian system of CRYOPAD. For a cubic system the rotation operation is $\vec{M}(\vec{Q})_{xyz} = P_{abc \rightarrow xyz}^{-1} \cdot \vec{M}(\vec{Q})_{abc}$, with $P_{abc \rightarrow xyz} = (\hat{x}, \hat{x} \times \hat{z}, \hat{z})$. For a given reflection, $\vec{M}(\vec{Q})_{\perp xyz}$ is then calculated for the different trial structures, with the corresponding nuclear structure factor $N = \sum_j \bar{b}_j \exp(i\vec{Q} \cdot \vec{r}_j)$, where the sum is over all j atoms in the unit cell and \bar{b}_j is the relevant scattering cross section, using previously determined crystallographic parameters [17].

The incoming polarization, \vec{P}_i , is substituted into the Blume–Maleev equations for analysis [18–20]. Omitting the \vec{Q} dependence of $\vec{M}(\vec{Q})_\perp$ for clarity:

$$\sigma = (NN^*) + (i\vec{P}_i \cdot (\vec{M}_\perp^* \times \vec{M}_\perp)) + (\vec{M}_\perp \cdot \vec{M}_\perp^*) + (\vec{P}_i \cdot (\vec{M}_\perp N^* + \vec{M}_\perp^* N)) \quad (2)$$

$$\begin{aligned} \vec{P}_f \sigma = & (\vec{P}_i NN^*) + (-i(\vec{M}_\perp^* \times \vec{M}_\perp)) \\ & + (-\vec{P}_i(\vec{M}_\perp \cdot \vec{M}_\perp^*) + \vec{M}_\perp(\vec{P}_i \cdot \vec{M}_\perp^*) + \vec{M}_\perp^*(\vec{P}_i \cdot \vec{M}_\perp)) \\ & + (N\vec{M}_\perp^* + N^*\vec{M}_\perp - i(N\vec{M}_\perp^* - N^*\vec{M}_\perp) \times \vec{P}_i). \end{aligned} \quad (3)$$

The basis vectors of four irreps, $\Gamma_{3,5,7,9}$, were calculated with the program SARAh [16]. The XY anisotropy is minimized by using either a linear combination of the basis vectors $\vec{\psi}_{2,3}$ that transform as the second order Γ_5 or the discrete set of symmetry equivalent basis vectors $\vec{\psi}_{4,5,6}$ that transform as the third order Γ_7 (see table 1).

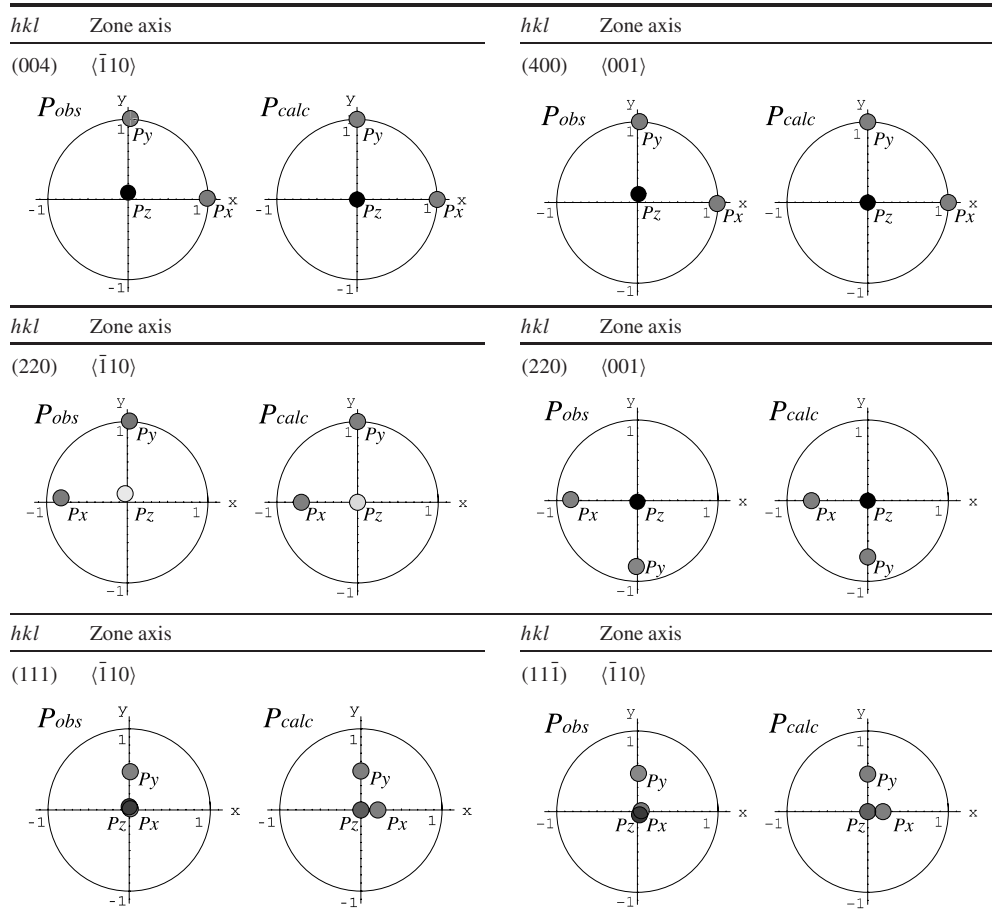
SNP provides a great deal of information about magnetic ordering in complex systems with the only data loss being due to magnetic domains [15]. For $\vec{k} = 0$ there can be one K-domain and only S-domains need be considered. These arise when the symmetry of the magnetic structure is less than the crystallographic one and regions form with rotationally related magnetic structures. Symmetry analysis indicates that there are six possible S-domains for Γ_5 , related by time-normal and time-reversed C_3 rotations. The polarization for each of these n S-domains needs to be calculated separately and summed, $\vec{P}_{f\text{dom}} = \sum_n \vec{P}_{fn} \sigma$. The experimental matrices were diagonal within error, a depolarization that is characteristic of time-reversed S-domains.

The $hh\bar{l}_{\text{odd}}$ reflections have matrices described by $P_{xx} < P_{yy} < P_{zz}$, implying that the magnetic interaction vector is mostly in the y and z direction. For the subset of $hh\bar{l}$ reflections, $hh\bar{l}_{\text{even}}$, $P_{xx} \approx P_{zz} < P_{yy}$, showing that the polarization is mostly parallel to the y direction. The set of $hk0$ reflections have diagonal matrix elements: $P_{xx} \approx P_{yy} < P_{zz}$; this shows that the magnetic interaction vector is mostly parallel to z and thus the $\langle 001 \rangle$ direction. The reflections $0k0$, $00l$ and $h0l$, $h = 4n$, $l = 4m$, have diagonal elements $P_{xx} \approx P_{yy} \approx P_{zz} \approx 1$, indicating that their magnetic interaction vectors are zero (see table 2).

The null magnetic structure factors for the $0k0$ and $00l$ reflections demonstrate that the magnetic structure is antiferromagnetic with the sum over the moments on the tetrahedron equal to zero: $\vec{M}(0k0) \propto \vec{M}(00l) \propto \sum \vec{m}_j = 0$.

Inspection of Γ_5 and Γ_7 reveals that the sum of the basis vectors $\vec{\psi}_{2,3}$ on the sites m_2 and m_3 , within Γ_5 , will give a magnetic component along the $\langle 001 \rangle$ or \vec{c} axis of the crystal, but not along the \vec{a} or \vec{b} axes. As combination of basis vectors within Γ_7 cannot produce this result, the magnetic ordering must be described by Γ_5 .

Table 2. The experimental and fitted values of the polarization vector for several characteristic reflections with the $\langle 1\bar{1}0 \rangle$ and $\langle 001 \rangle$ axes perpendicular. Dark circles indicate that the polarization is above the xy plane, and light circles that it is below.



The hhl_{odd} reflections generate two magnetic structure factors: $\vec{M}(\vec{Q}) = -2(\vec{m}_1)$ and $\vec{M}(\vec{Q}) = -2(\vec{m}_1 + \vec{m}_2 + \vec{m}_3) = 2\vec{m}_4$. The final polarization matrices are the same for equivalent reflections with either \vec{m}_1 or \vec{m}_4 contributing to the magnetic structure factor. Further observations are difficult as the magnetic interaction vector has both y and z components. One point to note is that the $(1, 1, 1)$ and $(1, 1, \bar{1})$ reflections are the strongest magnetic reflections of the hhl_{odd} set. These reflections give equivalent final polarization output (see table 2) and are described by $\vec{M}(\vec{Q}) = -2(\vec{m}_1)$ and $\vec{M}(\vec{Q}) = 2(\vec{m}_4)$ respectively. As expected for this $\langle 111 \rangle XY$ system, the moments on \vec{m}_1 and \vec{m}_4 lie in the planes perpendicular to the $\langle 111 \rangle$ and $\langle 111 \rangle$ directions respectively.

Refinement of the $c_{2,3}$ coefficients was carried out by minimizing the absolute difference, R , between the experimental and calculated values of P_f , $R = \frac{1}{N-1-v} \sum_N (P_{f\text{expt}} - P_{f\text{calc}})^2$, where the number of parameters $v = 1$. The same goodness of fit values were found for the coefficients $c_2 = 1.00(9)$, $c_3 = 0.00(9)$; $c_2 = 0.37(7)$, $c_3 = 0.63(7)$; $c_2 = -0.37(7)$, $c_3 = 0.63(7)$ and their sign inverted counterparts. As three solutions are related by C_3 rotations (see figure 2); the six possible solutions correspond to the six domains allowed within Γ_5 : three rotationally related domains and their time-reversed anti-domains.

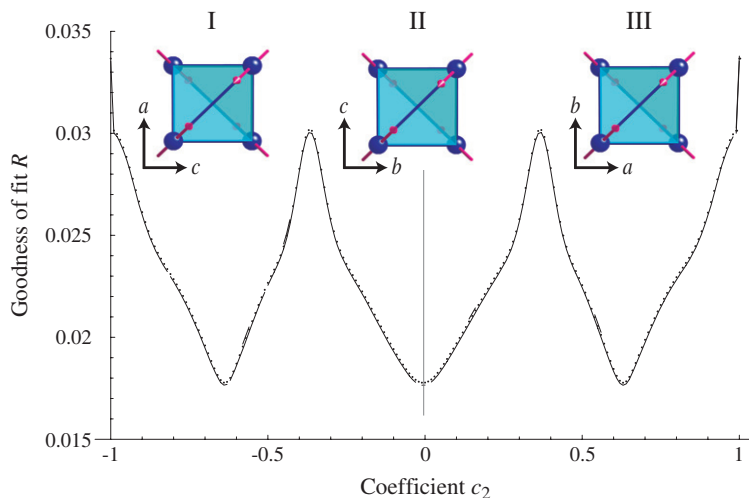


Figure 2. The goodness of fit as a function of the coefficient C_2 [21], where $\sum_i |C_i| = 1$ as described in the text, and the orientations of the moments that correspond to the labelled minima.

The SNP experiment further evidences $\text{Er}_2\text{Ti}_2\text{O}_7$ as a good model $\langle 111 \rangle XY$ pyrochlore antiferromagnet. The observed magnetic ordering, under $\vec{\psi}_2$ of Γ_5 , has been predicted to occur when quantum fluctuations break the degeneracy of $\vec{\psi}_{2,3}$ linear combination and so stabilize the magnetic ordering process. The refined moment was $\mu = 3.25(9) \mu_B$ which further supports the presence of large quantum fluctuations and correspondingly their importance, in this highly frustrated magnet. Our results go further, indicating that the microscopic magnetic structure is formed from six spin domains, all of which are equally occupied.

We thank the Royal Society and EPSRC for financial support and the DFRL for provision of a studentship. The authors would like to thank J D M Champion, P Holdsworth, and P J Brown for many interesting discussions.

References

- [1] Anderson P W 1973 *Mater. Res. Bull.* **8** 153
- [2] Villain J 1979 *Z. Phys. B* **33** 31
- [3] Harris M J *et al* 1997 *Phys. Rev. Lett.* **79** 2554
- [4] Ballou R, Lelièvre-Berna E and Fåk B 1996 *Phys. Rev. Lett.* **77** 790
- [5] Wills A S, Raju N P, Morin C and Greedan J E 1999 *Chem. Mater.* **11** 1936
- [6] Wills A S *et al* 1998 *Europhys. Lett.* **42** 325
- [7] Wills A S, Depuis V, Vincent E and Calemzuk R 2000 *Phys. Rev. B* **62** 9264(R)
- [8] Urano C *et al* 2000 *Phys. Rev. Lett.* **85** 1052
- [9] Champion J D M *et al* 2001 *Phys. Rev. B* **64** 140407
- [10] Stewart J R, Ehlers G, Wills A S, Bramwell S T and Gardner J S 2004 *J. Phys.: Condens. Matter* **16** L321
- [11] Bloemberger H W J *et al* 1969 *Physica* **43** 549
- [12] Champion J D M *et al* 2003 *Phys. Rev. B* **68** 020401(R)
- [13] Kovalev O V 1993 *Representations of the Crystallographic Space Groups* 2nd edn (Switzerland: Gordon and Breach)
- [14] Lelièvre-Berna E *et al* 1999 *Physica B* **397** 120–4
- [15] Brown P J, Forsyth B J and Tasset F 1993 *Proc. R. Soc. A* **442** 147–60
- [16] Wills A S 2000 *Physica B* **276** 680–1 (program available from www CCP14.ac.uk)
- [17] Dee A, Wills A S, Fernandez Diaz M T and Lelièvre-Berna E 2007 unpublished work
- [18] Izumov Y and Maleyev S 1962 *Sov. Phys.—JETP* **14** 1668
- [19] Blume M 1963 *Phys. Rev.* **130** 1670
- [20] Blume M 1963 *Phys. Rev.* **133** A1366
- [21] Wills A S 2001 *Phys. Rev. B* **63** 064430